Journal of Applied Fluid Mechanics, Vol. 9, No. 4, pp. 1591-1601, 2016.
Available online at www.jafmonline.net, ISSN 1735-3572, EISSN 1735-3645.
DOI: 10.18869/acadpub.jafm.68.235.25114

Steady State Analysis of Natural Convective Flow over a Moving Vertical Cylinder in the Presence of Porous Medium

P. Loganathan† and B. Eswari

Department of Mathematics, Anna University, Chennai-600 025, Tamil Nadu, India.

†*Corresponding Author Email: logu@annauniv.edu*

(Received May 27, 2015; accepted August, 23, 2015)

ABSTRACT

A numerical study is carried out for a free convection flow past a continuously moving semi-infinite vertical cylinder in the presence of porous medium. The governing boundary layer equations are converted into a non-dimensional form and then they are solved by an efficient, accurate and unconditionally stable implicit finite difference scheme of Crank-Nicolson method. Stability and convergence of the finite difference scheme are established. The velocity, temperature and concentration profiles have been presented for various parameters such as Prandtl number, Schmidt number, thermal Grashof number, mass Grashof number and permeability of the porous medium. The local as well as average skin-friction, Nusselt number and Sherwood number are also shown graphically. It is observed that the increase in the permeability parameter leads to increase in velocity profile, local as well as average shear stress, Nusselt number and Sherwood number but leads to decrease in temperature and concentration profiles. The results of temperature and concentration profiles are compared with available result in literature and are found to be in good agreement.

Keywords: Vertical cylinder; Natural convection; Heat and mass transfer; Porous medium; Finite difference.

NOMENCLATURE

C	species concentration
Gr	thermal Grashof number
Gc	mass Grashof number
g	acceleration due to gravity
i	grid point along the X-direction
j	grid point along the R-direction
$\overline{Nu}$	dimensionless average Nusselt number
Nu_x	local Nusselt number
Pr	Prandtl number
R	dimensionless radial coordinate
r	radial coordinate
r_0	radius of cylinder
Sc	Schmidt number
$\overline{Sh}$	dimensionless average Sherwood number
Sh_x	dimensionless local Sherwood number
T	temperature
t	time
U, V	dimensionless velocity components in X, R directions respectively
u, v	velocity components in x, r directions respectively
X	dimensionless axial co-ordinate
x	axial co-ordinate measured vertically upward
α	thermal diffusivity
β	volumetric coefficient of thermal expansion
β^*	volumetric coefficient of expansion with concentration
υ	kinematic viscosity
ρ	density
$\overline{\tau}$	dimensionless average skin-friction
τ_x	dimensionless local skin-friction
λ^*	permeability of the porous medium
λ	dimensionless permeability
Δt	grid size in time
ΔR	grid size in radial direction
ΔX	grid size in axial direction

1. INTRODUCTION

The study of transport phenomenon in porous media has primarily been initiated by the research activity in geophysical systems and chemical engineering industry. Therefore, the subject of the transport phenomena through fluid-saturated porous media represents an important area of rapid growth in the contemporary heat transfer research. The study of transport phenomena in porous materials has attracted considerable attention and has been motivated by a broad range of engineering applications which includes agricultural applications, environmental applications, industrial applications, thermal conversion and storage systems. Agricultural applications: e.g. fermentation process in food industries, freeze drying of food products, grain storage, soil heating to increase the growing season, etc. Environmental applications: e.g. ground water pollution, ground water systems, storage of radioactive waste, water movement in geothermal reservoirs, etc. Industrial applications: e.g. artificial freezing of ground as a structural support and as a water barrier for construction and mining purposes, crude oil production and recovery systems, porous radiant burners (PRBs), post-accident heat removal (PAHR), solidification of castings, study of heat transfer phenomenon of buried electrical cables and transformer cables, fluidized bed combustion, etc. Thermal conversion and storage systems: e.g. catalytic reactors, geothermal systems, packed beds, fluidized bed, heat pipes, sensible, latent and thermochemical energy storage systems, etc.

Porous media can be used as an insulator (for all temperature ranges) and can be used as a heat transfer promoter for either sensible or latent heat transfer. This makes the porous media a kind of super material which promotes the idea of the super compact heat exchanges. Different transport models are available in the literature, which are used to model energy and momentum transport in porous media.

Bottemanne (1972) gave experimental results of pure and simultaneous heat and mass transfer by free convection about a vertical cylinder for $Pr = 0.71$, $Sc = 0.63$. The author showed that the results are in close agreement with the classical free convection boundary layer theory for a vertical flat plate. The diameter of the cylinder was chosen as sufficiently large so that only a small correction was needed to compare their experimental results with the theoretical solution for a flat plate. Kuiken (1974) solved the free convection boundary-layer flow along a semi-infinite isothermal vertical cylinder considering the case that the boundary layer is thick in comparison with the radius of the cylinder.

Minkowycz and Cheng (1976) analyzed free convective flow about a vertical cylinder embedded in a saturated porous medium, where surface temperature of the cylinder varies as a power function of distance from the leading edge. They found that the local similarity solutions are sufficiently accurate for all the practical purposes compared to local non-similarity models. Merkin (1977) considered the free convection boundary layer from a vertical cylinder embedded in a saturated porous medium. The author showed that numerical solution of the governing equations failed to predict the flow at large distances along the cylinder and a simple approximate method can better represent the whole flow region than the full numerical solution.

An analytical study is performed by Chen and Yuh (1980) to examine the combined heat and mass characteristics of natural convection along a vertical cylinder. The authors analyzed that for heating/diffusing conditions, the local wall shear stress, the local Nusselt number, and the local Sherwood number increase with the increase in the curvature of the cylinder. Raptis *et al*. (1981) considered a steady two-dimensional free convection and mass transfer flow of an incompressible viscous fluid through a porous medium bounded by a vertical infinite limiting surface with constant temperature and concentration. They observed that the velocity increases when the permeability of the porous medium increases and the porosity of the medium helps in reducing the rate of heat transfer.

A numerical solution for a free convective flow past a vertical semi-infinite flat plate embedded in a saturated porous medium with constant permeability subject to a prescribed non-uniform wall temperature or to a prescribed non-uniform wall heat flux was solved by Na and Pop (1983). Bejan and Khair (1985) studied the heat and mass transfer by natural convection near a vertical surface embedded in a fluid-saturated porous medium. The report contained both scale analysis and similarity formulation. They determined the scale analysis of heat and mass transfer rates for each regime.

The unsteady free convective flow through a porous medium when the temperature of the plate is oscillating with time about a constant nonzero mean was studied by Singh *et al*. (1986). They provided the solution for both small and large frequency parameters by developing two asymptotic expansion methods. They observed that the velocity increases significantly with the increase in the value of permeability of the porous medium.

Development of two-dimensional boundary layer with an applied magnetic field due to an impulsive motion was studied by Kumari and Nath (1999). The parabolic partial differential equations governing the unsteady flow have been solved numerically using an implicit finite difference scheme. Analytical solutions have also been obtained for some particular cases. Ganesan and Rani (2000) studied the natural convection on a vertical cylinder under the combined effects of heat and mass transfer along with the chemically reactive species. They studied both the generative and destructive reactions.

Unsteady three-dimensional MHD-boundary-layer flow due to the impulsive motion of a stretching

surface was studied by Takhar *et al*. (2001). The partial differential equations governing the unsteady laminar boundary-layer flow were solved numerically using an implicit finite difference scheme. For some particular cases, analytical solutions were obtained, and for large values of the independent variable asymptotic solutions were found. Ganesan and Loganathan (2001) considered the transient natural convection boundary layer flow of an incompressible viscous fluid past an impulsively started moving semi-infinite vertical cylinder. They observed that the skin friction values are negative at small values of Schmidt number and they are positive for larger values of Schmidt number showing that separation of flow may not occur at the cylinder.

Postelnicu (2004) numerically studied the heat and mass transfer characteristics of natural convection about a vertical surface embedded in a saturated porous medium subjected to a magnetic field taking into account Dufour and Soret effects. It was found that the increase in magnetic field parameter also increases the thickness of the hydrodynamic, thermal and concentration boundary layers. Akyildiz *et al.* (2006) considered diffusion of chemically reactive species of a non-Newtonian fluid immersed in a porous medium over a stretching sheet. They found that the thickness of the concentration boundary layer decreases with the reaction rate parameter. Patil and Kulkarni (2008) studied the effects of chemical reaction and internal heat generation on the free convective flow with heat and mass transfer of a polar fluid through porous medium in the presence of couple stresses. Cheng (2010) analysed the soret and dufour effects on the boundary layer flow due to free convection heat and mass transfer over a vertical cylinder in a porous medium saturated with Newtonian fluids with constant wall temperature and concentration.

The problem of unsteady MHD mixed convection heat and mass transfer near the stagnation point of a three dimensional porous body in the presence of heat generation/absorption and chemical reaction effects was studied by Chamkha and Ahmed (2011). They found that the increase in the value of magnetic field parameter, increases the skin-friction coefficients, temperature and solute concentration in the fluid but decreases the velocity components, Nusselt number and Sherwood number. Chamkha *et al*. (2011) analyzed the natural convection past a sphere embedded in a non-Darcy porous medium saturated by a nanofluid. The results indicated that as Buoyancy ratio and Thermophoresis parameter increase, the friction factor increases, whereas there is a decrease in heat transfer rate and mass transfer rate.

An analysis has been made to study the steady axi-symmetric flow of an incompressible viscous fluid along a vertical stretching cylinder in porous medium by Mukhopadhyay (2012). The results pertaining to the study indicated that due to increasing values of permeability parameter, velocity decreases and the temperature increases. Also the rate of transport has been considerably reduced with increasing values of curvature parameter. The heat and mass transfer analysis for boundary layer stagnation-point flow over a stretching sheet in a porous medium saturated by a nanofluid with internal heat generation/absorption and suction/blowing has been investigated by Hamad and Ferdows (2012). Using group-theoretical methods, they obtained the similarity solutions through Lie group analysis.

Mukhopadhyay and Ishak (2012) considered the steady axisymmetric mixed convection flow of an incompressible viscous fluid along a stretching cylinder embedded in a thermally stratified fluid-saturated medium of variable ambient temperature. Similarity transformation is employed to convert the governing partial differential equations into highly nonlinear ordinary differential equations. The analysis of their results obtained showed that the flow field was influenced appreciably by the mixed convection parameter and the thermal stratification parameter. Numerical solutions to the unsteady convective boundary layerflow of a viscous fluid at a vertical stretching surface with variable transport properties and thermal radiation are given by Vajravelu *et al*. (2013). It was found that the momentum and thermal boundary layer thickness decrease with an increase in the unsteady parameter.

Ashorynejad *et al*. (2013) investigated the heat transfer of a nanofluid over a stretching cylinder in the presence of magnetic field. It was found that the effect of transverse magnetic field suppresses the velocity field, which in turn causes the enhancement of the temperature field. Rohni *et al*. (2013) considered a steady, axisymmetric boundary-layer flow along a vertical cylinder embedded in a porous medium filled with a nanofluid. The effects of variable viscosity and thermal conductivity on the natural convection heat transfer over a vertical plate embedded in a porous medium saturated by a nanofluid are investigated by Noghrehabadi *et al*. (2014). It was concluded that the concentration gradient of nanoparticles due to thermophoresis and Brownian motion forces affects the local viscosity and thermal conductivity of nanofluids and consequently affects the heat transfer of nanofluids.

Numerical solution of MHD fluid flow and heat transfer characteristics of a viscous incompressible fluid along a continuously stretching horizontal cylinder embedded in a porous medium in the presence of internal heat generation or absorption was carried out by Yadav and Sharma (2014). Fluid temperature increases due to increase in permeability parameter, magnetic parameter, heat generation parameter or curvature parameter with the decrease in fluid velocity. A numerical investigation of two-dimensional steady laminar free convection flow with heat and mass transfer past a moving vertical plate in a porous medium subjected to a transverse magnetic field has been carried out by Javaherdeh *et al*. (2015). They found that the higher value of the porosity parameter leads to the reduction in velocity which is accompanied by a reduction in both Nusselt and Sherwood number.

An analytical study has been performed on the MHD flow and thermal transport characteristics of nanofluid flow past a vertical porous plate with a radiation effect in a rotating system by Narayana *et al*. (2015). The authors found that the velocity profile decreases with an increase in nanoparticle volume fraction, while the opposite is true in the case of temperature profiles. Also it was found that the radiation has a greater influence on both the thermal boundary layer thickness and the nanoparticle volume fraction profiles.

The objective of present investigation is to study the natural convective flow of an incompressible viscous fluid over moving semi-infinite vertical cylinder with heat and mass transfer in the presence of porous medium. In this analysis, the cylinder is moving in the vertical direction against gravitational force with a uniform velocity u_0. The governing boundary layer equations along with the initial and boundary conditions are transformed into a dimensionless form and the resulting equations are solved by a semi-implicit finite difference scheme of the Crank – Nicolson type.

2. MATHEMATICAL ANALYSIS

Consider the free convection flow of a viscous incompressible, laminar flow over an impulsively moving semi infinite vertical cylinder of radius r_0. Initially both cylinder and the fluid are stationary at the same temperature T'_∞ and also at the same concentration level C'_∞. At a time $t' \geq 0$, the cylinder starts moving in the vertical direction with uniform velocity u_0. The temperature and the concentration on the surface of the cylinder are also raised to T'_w and C'_w. The effect of viscous dissipation is assumed to be negligible. The axial and radial co-ordinates are taken to be x and r, with x-axis measured vertically upward along the axis of the cylinder and r-axis measured normal to axis of cylinder. Under these assumptions, the governing boundary layer equations of continuity, momentum, energy and species concentration with Boussisnesq's approximation are as follows (Velusamy and Garg 1992):

$$\frac{\partial}{\partial x}(ru) + \frac{\partial}{\partial r}(rv) = 0 \tag{1}$$

$$\frac{\partial u}{\partial t'} + u\frac{\partial u}{\partial x} + v\frac{\partial u}{\partial r} = g\beta\left(T' - T'_\infty\right) + g\beta^*\left(C' - C'_\infty\right) + \frac{\upsilon}{r}\frac{\partial}{\partial r}\left(r\frac{\partial u}{\partial r}\right) - \frac{\upsilon}{\lambda^*}u \tag{2}$$

$$\frac{\partial T'}{\partial t'} + u\frac{\partial T'}{\partial x} + v\frac{\partial T'}{\partial r} = \frac{\alpha}{r}\frac{\partial}{\partial r}\left(r\frac{\partial T'}{\partial r}\right) \tag{3}$$

$$\frac{\partial C'}{\partial t'} + u\frac{\partial C'}{\partial x} + v\frac{\partial C'}{\partial r} = \frac{D}{r}\frac{\partial}{\partial r}\left(r\frac{\partial C'}{\partial r}\right) \tag{4}$$

The initial and boundary conditions are

$$\begin{aligned} &t' \leq 0 : u = 0,\ v = 0,\ T' = T'_\infty,\ C' = C'_\infty\ \forall\ x \geq 0, r \geq 0 \\ &t' > 0 : u = u_0,\ v = 0,\ T' = T'_w,\ C' = C'_w \text{ at } r = r_0 \\ &\qquad u = 0,\ T' = T'_\infty,\ C' = C'_\infty \text{ at } x = 0, r \geq 0 \\ &\qquad u \to 0,\ T' \to T'_\infty,\ C' \to C'_\infty \text{ as } r \to \infty \end{aligned} \tag{5}$$

Introducing the following non-dimensional quantities

$$\begin{aligned} &X = \frac{x\upsilon}{u_0 r_0^2},\ R = \frac{r}{r_0},\ U = \frac{u}{u_0},\ V = \frac{vr_0}{\upsilon},\ t = \frac{t'\upsilon}{r_0^2}, \\ &T = \frac{T' - T'_\infty}{T'_w - T'_\infty},\ C = \frac{C' - C'_\infty}{C'_w - C'_\infty},\ Gr = \frac{g\beta r_0^2\left(T'_w - T'_\infty\right)}{\upsilon u_0}, \\ &Gc = \frac{g\beta^* r_0^2\left(C'_w - C'_\infty\right)}{\upsilon u_0},\ Sc = \frac{\upsilon}{D},\ \Pr = \frac{\upsilon}{\alpha},\ \lambda = \frac{\lambda^*}{r_0^2} \end{aligned} \tag{6}$$

Equations (1) – (4) are reduced to the following non dimensional form:

$$\frac{\partial(RU)}{\partial X} + \frac{\partial(RV)}{\partial R} = 0 \tag{7}$$

$$\frac{\partial U}{\partial t} + U\frac{\partial U}{\partial X} + V\frac{\partial U}{\partial R} = GrT + GcC + \frac{1}{R}\frac{\partial}{\partial R}\left(R\frac{\partial U}{\partial R}\right) - \frac{1}{\lambda}U \tag{8}$$

$$\frac{\partial T}{\partial t} + U\frac{\partial T}{\partial X} + V\frac{\partial T}{\partial R} = \frac{1}{\Pr R}\frac{\partial}{\partial R}\left(R\frac{\partial T}{\partial R}\right) \tag{9}$$

$$\frac{\partial C}{\partial t} + U\frac{\partial C}{\partial X} + V\frac{\partial C}{\partial R} = \frac{1}{ScR}\frac{\partial}{\partial R}\left(R\frac{\partial C}{\partial R}\right) \tag{10}$$

The corresponding initial and boundary conditions in non-dimensional quantities are given by

$$\begin{aligned} &t \leq 0 :\ U = 0,\ V = 0,\ T = 0,\ C = 0\ \ \forall\ X \geq 0,\ R \geq 0 \\ &t > 0 :\ U = 1,\ V = 0,\ T = 1,\ C = 1 \text{ at } R = 1 \\ &\qquad U = 0,\ T = 0,\ C = 0 \text{ at } X = 0 \text{ and } R \geq 1 \\ &\qquad U \to 0,\ T \to 0,\ C \to 0 \text{ as } R \to \infty \end{aligned} \tag{11}$$

3. NUMERICALTECHNIQUE

In order to solve the unsteady, non-linear coupled Eqs.(7) – (10) under the condition (11), an implicit finite difference scheme of Crank-Nicolson type described by Ganesan and Loganathan (2001) is employed. The region of integration is considered as a rectangle with sides $\mathrm{X}_{\max}(=1.0)$ and $\mathrm{R}_{\max}(=15.0)$ where $\mathrm{R}_{\max}$ corresponds to $\mathrm{R} \to \infty$ which lies very well outside the momentum, thermal and concentration boundary layers. The finite difference equations corresponding to Eqs. (7) to (10) are:

$$\frac{\left(\begin{matrix} U^{m+1}_{i,j-1} - U^{m+1}_{i-1,j-1} + U^{m+1}_{i,j} - U^{m+1}_{i-1,j} + \\ U^{m}_{i,j-1} - U^{m}_{i-1,j-1} - U^{m}_{i,j} - U^{m}_{i-1,j} \end{matrix}\right)}{4\Delta X} + \frac{V^{m+1}_{i,j} - V^{m+1}_{i,j-1} + V^{m}_{i,j} - V^{m}_{i,j-1}}{2\Delta R} + \frac{V^{m+1}_{i,j}}{1 + (j-1)\Delta R} = 0 \tag{12}$$

$$\frac{U_{i,j}^{m+1}-U_{i,j}^{m}}{\Delta t}+U_{i,j}^{m}\frac{\left(U_{i,j}^{m+1}-U_{i-1,j}^{m+1}+U_{i,j}^{m}-U_{i-1,j}^{m+1}\right)}{2\Delta X}+V_{i,j}^{m}\frac{\left(U_{i,j+1}^{m+1}-U_{i,j-1}^{m+1}+U_{i,j+1}^{m}-U_{i,j-1}^{m}\right)}{4\Delta R}=Gr\left(\frac{T_{i,j}^{m+1}+T_{i,j}^{m}}{2}\right)+Gc\left(\frac{C_{i,j}^{m+1}+C_{i,j}^{m}}{2}\right)+\frac{\left(U_{i,j-1}^{m+1}-2U_{i,j}^{m+1}+U_{i,j+1}^{m+1}+U_{i,j-1}^{m}-2U_{i,j}^{m}-U_{i,j+1}^{m}\right)}{2\left(\Delta R\right)^{2}}+\frac{\left(U_{i,j+1}^{m+1}-U_{i,j-1}^{m+1}+U_{i,j+1}^{m}-U_{i,j-1}^{m}\right)}{4\left(1+\left(j-1\right)\Delta R\right)\Delta R}-\frac{1}{\lambda}\left(\frac{U_{i,j}^{m+1}+U_{i,j}^{m}}{2}\right) \tag{13}$$

$$\frac{T_{i,j}^{m+1}-T_{i,j}^{m}}{\Delta t}+U_{i,j}^{m}\frac{\left(T_{i,j}^{m+1}-T_{i-1,j}^{m+1}+T_{i,j}^{m}-T_{i-1,j}^{m+1}\right)}{2\Delta X}+V_{i,j}^{m}\frac{\left(T_{i,j+1}^{m+1}-T_{i,j-1}^{m+1}+T_{i,j+1}^{m}-T_{i,j-1}^{m}\right)}{4\Delta R}=\frac{\left(T_{i,j-1}^{m+1}-2T_{i,j}^{m+1}+T_{i,j+1}^{m+1}+T_{i,j-1}^{m}-2T_{i,j}^{m}-T_{i,j+1}^{m}\right)}{2\,\mathrm{Pr}\left(\Delta R\right)^{2}}+\frac{\left(T_{i,j+1}^{m+1}-T_{i,j-1}^{m+1}+T_{i,j+1}^{m}-T_{i,j-1}^{m}\right)}{4\,\mathrm{Pr}\left(1+\left(j-1\right)\Delta R\right)\Delta R} \tag{14}$$

$$\frac{C_{i,j}^{m+1}-C_{i,j}^{m}}{\Delta t}+U_{i,j}^{m}\frac{\left(C_{i,j}^{m+1}-C_{i-1,j}^{m+1}+C_{i,j}^{m}-C_{i-1,j}^{m+1}\right)}{2\Delta X}+V_{i,j}^{m}\frac{\left(C_{i,j+1}^{m+1}-C_{i,j-1}^{m+1}+C_{i,j+1}^{m}-C_{i,j-1}^{m}\right)}{4\Delta R}=\frac{\left(C_{i,j-1}^{m+1}-2C_{i,j}^{m+1}+C_{i,j+1}^{m+1}+C_{i,j-1}^{m}-2C_{i,j}^{m}-C_{i,j+1}^{m}\right)}{2Sc\left(\Delta R\right)^{2}}+\frac{\left(C_{i,j+1}^{m+1}-C_{i,j-1}^{m+1}+C_{i,j+1}^{m}-C_{i,j-1}^{m}\right)}{4Sc\left(1+\left(j-1\right)\Delta R\right)\Delta R} \tag{15}$$

Here i-designates X-direction $i\Delta X$, j-designates R-direction $1+\left(j-1\right)\Delta R$ and the superscript m designates a value of time $m\Delta t$. During any one-time step, the coefficients $U_{i,j}^{m}$ and $V_{i,j}^{m}$ appearing in Eqs. (12) – (15) are treated as constants. The value of *U*, *V*, *T* and *C* are known at time $t=0$ from the initial conditions. The values of *C*, *T*, *V* and *U* at the next time step $t=\Delta t$ are calculated as follows:

Equation (15) at every internal nodal point on a particular *i*-level constitutes a tri-diagonal system of equations which is solved by Thomas algorithm, described by Carnahan *et al*. (1969). Thus, the values of *C* are known at every nodal point on a particular *i*-level at $t=\Delta t$. Similarly, the values of *T* are calculated from Eq. (14). Using the values of *C* and *T* in Eq. (13), the values of *U* are calculated. Then the values of *V* are calculated explicitly by using Eq. (12) at every nodal point on a particular *i*-level. After computing the values corresponding to each *i* at a time level, the values of the next time are determined similarly.

After experimenting with few sets of mesh sizes, the mesh sizes have been fixed at the level $\Delta\mathrm{X}=0.02$, $\Delta\mathrm{R}=0.2$ with time step $\Delta t=0.01$. In this case, spatial mesh sizes are reduced by 50% in one direction, and later in both directions, and results are compared. It is observed that, when the mesh size is reduced by 50% in the R-direction, the results differ in the fifth place after the decimal point while the mesh sizes are reduced by 50% in X-direction or in both directions the results are correct to five decimal places. Hence, the above mesh sizes have been considered as appropriate for calculation.

This iterative procedure is repeated for many time steps until the steady-state solution is reached. The steady-state solution is assumed to have been reached, when the absolute difference between the values of velocity *U*, temperature *T* as well as concentration *C*at two consecutive time steps are less than 10^{-5} at all grid points.

4. STABILITY AND CONVERGENCE OF THE FINITE DIFFERENCE SCHEME

The criterion of the finite difference scheme for constant mesh size is examined using Von-Neumann technique as follows:

The general term of the Fourier expansion for U, T and C at a time arbitrarily called $t=0$ are assumed to be $e^{i\alpha X}e^{i\beta R}$. At a later time t these terms will become

$$\begin{aligned}U&=F\left(t\right)e^{i\alpha X}e^{i\beta R}\\T&=G\left(t\right)e^{i\alpha X}e^{i\beta R}\\C&=H\left(t\right)e^{i\alpha X}e^{i\beta R}\end{aligned} \tag{16}$$

Substituting (16) in (13)–(15) under the assumptions that the coefficients *U*, *T* and *C*are constants over any one time step and denoting the values after one time by F', G′ and H′. After simplification, we get

$$\frac{F'-F}{\Delta t}+\frac{U\left(F'+F\right)\left(1-e^{-i\alpha\Delta X}\right)}{2\Delta X}+\frac{V\left(F'+F\right)i\sin\left(\beta\Delta R\right)}{2\Delta R}=\frac{Gr\left(G'+G\right)}{2}+\frac{Gc\left(H'+H\right)}{2}+\frac{\left(F'+F\right)\left(\cos\left(\beta\Delta R\right)-1\right)}{\left(\Delta R\right)^{2}}+\frac{\left(F'+F\right)i\sin\left(\beta\Delta R\right)}{2\left(1+\left(j-1\right)\Delta R\right)\Delta R}-\frac{F'+F}{2\lambda} \tag{17}$$

$$\frac{G'-G}{\Delta t}+\frac{U\left(G'+G\right)\left(1-e^{-i\alpha\Delta X}\right)}{2\Delta X}+\frac{V\left(G'+G\right)i\sin\left(\beta\Delta R\right)}{2\Delta R}=\frac{\left(G'+G\right)\left(\cos\left(\beta\Delta R\right)-1\right)}{\mathrm{Pr}\left(\Delta R\right)^{2}}+\frac{\left(G'+G\right)i\sin\left(\beta\Delta R\right)}{2\,\mathrm{Pr}\left(1+\left(j-1\right)\Delta R\right)\Delta R} \tag{18}$$

$$\frac{H'-H}{\Delta t}+\frac{U\left(H'+H\right)\left(1-e^{-i\alpha\Delta X}\right)}{2\Delta X}+\frac{V\left(H'+H\right)i\sin\left(\beta\Delta R\right)}{2\Delta R}=\frac{\left(H'+H\right)\left(\cos\left(\beta\Delta R\right)-1\right)}{Sc\left(\Delta R\right)^2}+\frac{\left(H'+H\right)i\sin\left(\beta\Delta R\right)}{2Sc\left(1+\left(j-1\right)\Delta R\right)\Delta R} \tag{19}$$

Let us consider

$$A=\frac{U\left(1-e^{-i\alpha\Delta X}\right)\Delta t}{2\Delta X}+\frac{Vi\sin\left(\beta\Delta R\right)\Delta t}{2\Delta R}-\frac{\left(\cos\left(\beta\Delta R\right)-1\right)\Delta t}{\left(\Delta R\right)^2}-\frac{i\sin\left(\beta\Delta R\right)\Delta t}{2\left(1+\left(j-1\right)\Delta R\right)\Delta R}+\frac{\Delta t}{2\lambda}$$

$$B=\frac{U\left(1-e^{-i\alpha\Delta X}\right)\Delta t}{2\Delta X}+\frac{Vi\sin\left(\beta\Delta R\right)\Delta t}{2\Delta R}-\frac{\left(\cos\left(\beta\Delta R\right)-1\right)\Delta t}{\Pr\left(\Delta R\right)^2}-\frac{i\sin\left(\beta\Delta R\right)\Delta t}{2\Pr\left(1+\left(j-1\right)\Delta R\right)\Delta R}$$

$$C=\frac{U\left(1-e^{-i\alpha\Delta X}\right)\Delta t}{2\Delta X}+\frac{Vi\sin\left(\beta\Delta R\right)\Delta t}{2\Delta R}-\frac{\left(\cos\left(\beta\Delta R\right)-1\right)\Delta t}{Sc\left(\Delta R\right)^2}-\frac{i\sin\left(\beta\Delta R\right)\Delta t}{2Sc\left(1+\left(j-1\right)\Delta R\right)\Delta R} \tag{20}$$

Substituting A, B and C in Eqs. (17) – (19), we get

$$\left(1+A\right)F'=\left(1-A\right)F+\frac{Gr\left(G'+G\right)\Delta t}{2}+\frac{Gc\left(H'+H\right)\Delta t}{2} \tag{21}$$

$$\left(1+B\right)G'=\left(1-B\right)G \tag{22}$$

$$\left(1+C\right)H'=\left(1-C\right)H \tag{23}$$

Equations (21) – (23) can be written in the matrix form as follows:

$$\begin{bmatrix}F'\\G'\\H'\end{bmatrix}=\begin{bmatrix}\frac{1-A}{1+A} & D_1 & D_2\\ 0 & \frac{1-B}{1+B} & 0\\ 0 & 0 & \frac{1-C}{1+C}\end{bmatrix}\begin{bmatrix}F\\G\\H\end{bmatrix} \tag{24}$$

where $D_1=\frac{\Delta t\ Gr}{\left(1+A\right)\left(1+B\right)}, D_2=\frac{\Delta t\ Gc}{\left(1+A\right)\left(1+C\right)}$.

For stability of the finite difference scheme, the modulus of each eigen value of an amplification matrix must not exceed unity. The Eigen values of the amplification matrix are given by (1–A)/(1+A), (1–B)/(1+B) and(1–C)/(1+C). Considering U everywhere positive and V everywhere negative and let

$$A=2a\sin^2\left(\alpha\Delta X/2\right)+2d\sin^2\left(\beta\Delta R/2\right)+\frac{\Delta t}{2\lambda}+ia\sin\left(\alpha\Delta X\right)+i\left(b-c\right)\sin\left(\beta\Delta R\right)$$

where $a=\frac{U\Delta t}{2\Delta X},\ b=\frac{V\Delta t}{2\Delta R},\ c=\frac{\Delta t}{2\left(1+\left(j-1\right)\Delta R\right)\Delta R},\ d=\frac{\Delta t}{\left(\Delta R\right)^2}$

$$B=2a\sin^2\left(\alpha\Delta X/2\right)+2d\sin^2\left(\beta\Delta R/2\right)+ia\sin\left(\alpha\Delta X\right)+i\left(b-c\right)\sin\left(\beta\Delta R\right)$$

where $a=\frac{U\Delta t}{2\Delta X},\ b=\frac{V\Delta t}{2\Delta R},\ c=\frac{\Delta t}{2\Pr\left(1+\left(j-1\right)\Delta R\right)\Delta R},\ d=\frac{\Delta t}{\Pr\left(\Delta R\right)^2}$

$$C=2a\sin^2\left(\alpha\Delta X/2\right)+2d\sin^2\left(\beta\Delta R/2\right)+ia\sin\left(\alpha\Delta X\right)+i\left(b-c\right)\sin\left(\beta\Delta R\right)$$

where $a=\frac{U\Delta t}{2\Delta X},\ b=\frac{V\Delta t}{2\Delta R},\ c=\frac{\Delta t}{2Sc\left(1+\left(j-1\right)\Delta R\right)\Delta R},\ d=\frac{\Delta t}{Sc\left(\Delta R\right)^2}$

Since the real part of A is greater than or equal to zero, $\left|\left(1-A\right)/\left(1+A\right)\right|\le 1$ always. Similarly $\left|\left(1-B\right)/\left(1+B\right)\right|\le 1$ and $\left|\left(1-C\right)/\left(1+C\right)\right|\le 1$.

Therefore the scheme is unconditionally stable. The local truncation error is $O\left(\Delta t^2+\Delta R^2+\Delta X\right)$ and it tends to zero as Δt, ΔR and ΔX tend to zero. Hence the scheme is compatible. The stability and compatibility ensures the convergence of the finite difference scheme.

5. RESULTS AND DISCUSSION

The problem of free convective flow past a continuously moving semi-infinite vertical cylinder is considered in the presence of a porous medium. The equations are solved numerically by employing a finite difference scheme and the results are presented graphically.

In order to assess the accuracy of our method, the finite difference solution of temperature and concentration profiles for the stationary cylinder $Pr=0.7$, $Sc=0.6$, $Gr = Gc = 2.0$, $\lambda = 0$ (corresponding to $\xi=0$) are compared with the results of Chen and Yuh (1980). Figure 1 shows that there is an excellent match between the two solutions.

Figures 2 to 6 depicts the transient velocity, temperature and concentration profiles for different values of physical parameters such as *Sc* = 0.16, 0.6 and 2, *Pr* = 0.71 (air) and *Pr* = 7.0 (water), *Gr* and *Gc*. The profiles presented are those at $X=1.0$.

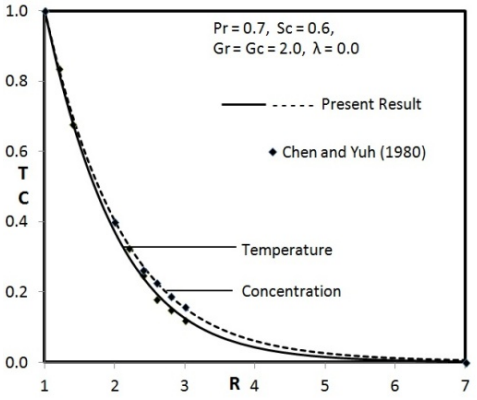

Fig. 1. Comparison of temperature and concentration profile.

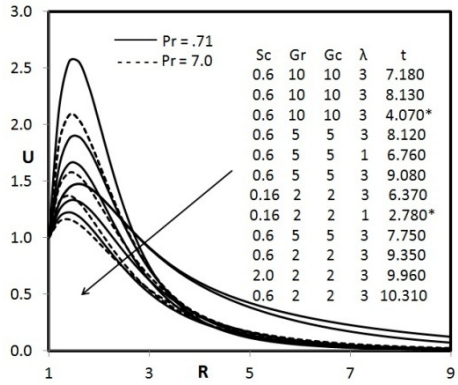

Fig. 2. Transient velocity profiles at X = 1.0 for different values of *Sc*, *Gr*, *Gc* and λ (* - temporal maximum).

The transient velocity profiles for different values of *Pr*, *Gr*, *Gc*, *Sc* and λ against the radial coordinate *R* are shown in Fig. 2. Permeability is the capacity of a porous material to allow fluids to pass through it depending on the number, geometry and size of interconnected pores. It can be seen that increase in λ leads to increase in the velocity profiles. It is observed that the time required to reach the steady state is less compared to higher value of λ. But the steady-state velocity decreases for increasing values of *Pr*. Increase in *Gr* and *Gc* reduces the time to reach the steady-state. The velocity profile increases for increasing values of *Gr* and *Gc*. The momentum boundary layer thickness increases with increasing values of *Gr*and *Gc*. Schmidt number physically relates the relative thickness of the hydrodynamic layer and mass-transfer boundary layer and thus the momentum boundary layer thickness increases for decreasing values of Sc.

From Fig. 3, it is clear that increase in λ leads to decrease in temperature profile. The thermal boundary layer thickness increases with decreasing values of λ. A temporal maximum is also observed. It can be seen that the temporal maximum is reached at an early stage for decreasing value of λ. The temperature profile increases for decreasing values of *Pr*. This is due to the fact that Prandtl number controls the relative thickness of the momentum and thermal boundary layers and when *Pr* is small, the heat diffuses quickly compared to the velocity boundary layer. This means the thickness of the thermal boundary layer is much bigger than the velocity boundary layer.

From Fig. 4, it is observed that temperature increases with decreasing values of *Gr* and *Gc*. The transient temperature profile increases steadily, reaches temporal maximum and after certain lapse of time attains the steady-state. Lower temperature profiles are observed for higher *Pr* or lower values of Sc. This is due to the fact that fluids with larger *Pr* give rise to less heat transfer. But the thermal boundary layer thickness increases with increasing *Sc*. The time taken to reach the steady-state is higher for higher values of *Pr*.

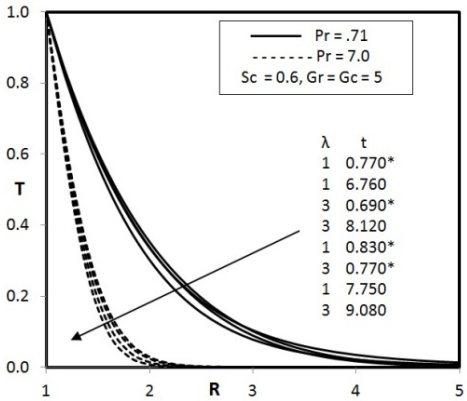

Fig. 3. Transient temperature profiles at X = 1.0 for different values of λ.

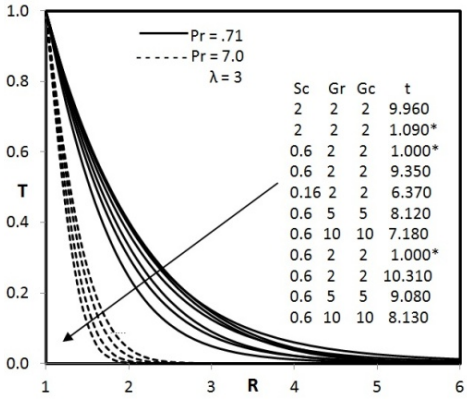

Fig. 4. Transient temperature profiles at X = 1.0 for different values of *Sc*, *Gr* and *Gc*.

From Fig. 5, it is clear that when the permeability λ increases, the concentration profile decreases. The concentration profile increases for increasing value of *Pr*. From Fig. 6, it is observed that concentration increases for decreasing values of *Gr*, *Gc* and *Sc*. The time taken to reach the steady-state is higher for higher value of *Pr*.

Knowing the velocity, temperature and

concentration profiles, it is interesting to study the local and average skin-friction, the rate of heat transfer and mass transfer both in the transient and steady-state.

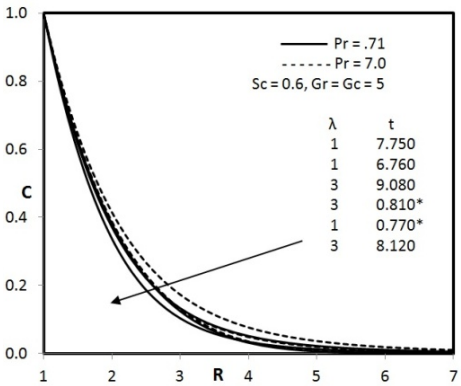

Fig. 5. Transient concentration profiles at X=1.0 for different values of λ.

The local as well as average skin-friction, Nusselt number and Sherwood number in terms of dimensionless quantities are given by

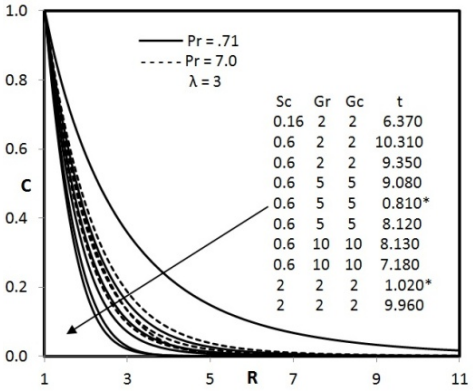

Fig. 6. Transient concentration profiles at X=1.0 for different values of λ.

$$\tau_X = -\left(\partial U/\partial R\right)_{R=1} \tag{25}$$

$$\tau = -\int_0^1 \left(\partial U/\partial R\right)_{R=1} \mathrm{dX} \tag{26}$$

$$Nu_X = -\frac{X\left(\partial T/\partial R\right)_{R=1}}{T_{R=1}} \tag{27}$$

$$\overline{Nu} = -\int_0^1 \frac{\left(\partial T/\partial R\right)_{R=1}}{T_{R=1}} \mathrm{dX} \tag{28}$$

$$Sh_X = -X\left(\partial C/\partial R\right)_{R=1} \tag{29}$$

$$\overline{Sh_X} = -\int_0^1 \left(\partial C/\partial R\right)_{R=1} dX \tag{30}$$

The derivatives involved in Eqs. (25)–(30) are evaluated using five-point approximation formula and integrals are evaluated using Newton-Cotes formula.

Local skin-friction τ_X profiles are plotted in Fig. 7 against the axial coordinate *X*. The local shear stress τ_X increases with increasing values of *Sc* and decreasing values of *Gr* and *Gc*. The shear stress increases as *Pr* increases. It is observed that the skin friction values are negative at small values of *Sc* indicating that separation of flow may occur at the cylinder and they are positive for larger values of *Sc* showing that separation of flow may not occur at the cylinder.

The local Nusselt number Nu_X for different values of *Gr*, *Gc*, *Sc* and λ are shown in Fig. 8. Local Nusselt number Nu_X increases with decreasing values of *Sc* and increasing values of *Gr* and *Gc*.

The local Sherwood number Sh_X increases with increasing values of *Gr* and *Gc* and the trend is just opposite with respect to *Sc* which is seen in Fig. 9. Increasing values of λ leads to increase in local shear stress, local heat transfer rate and local mass transfer rate. For larger values of *Pr*, there is an increase in local skin friction and local Nusselt number but the trend is just opposite in local Sherwood number.

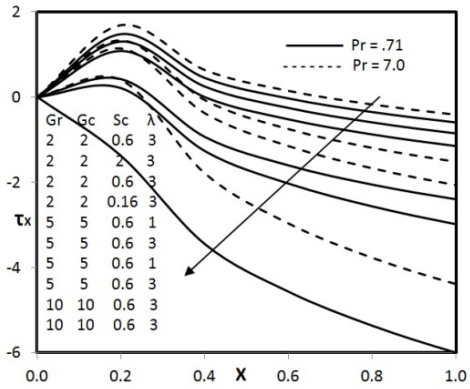

Fig. 7. Local skin friction.

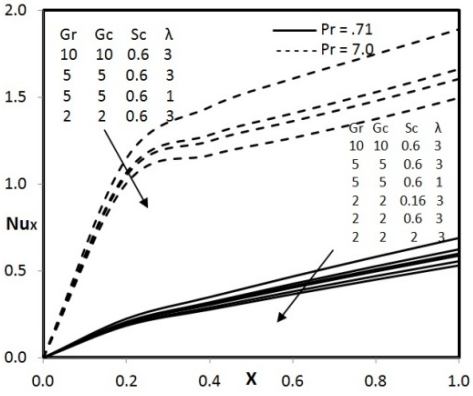

Fig. 8. Local Nusselt number.

The effects of *Gr*, *Gc*, *Sc* and λ on the average values of skin-friction $\overline{\tau}$, Nusselt number $\overline{\mathrm{Nu}}$ and

Sherwood number $\overline{Sh}$ are shown in Figs. 10– 12 respectively as a function of time for different values of physical parameters.

Figure 10 shows that rate of shear stress increases with increasing values of *Sc* and decreasing values of *Gr* and *Gc*. It is observed that average skin-friction increases with t and after certain lapse of time they are steady throughout the transient period. The rate of shear stress increases with increasing value of λ.

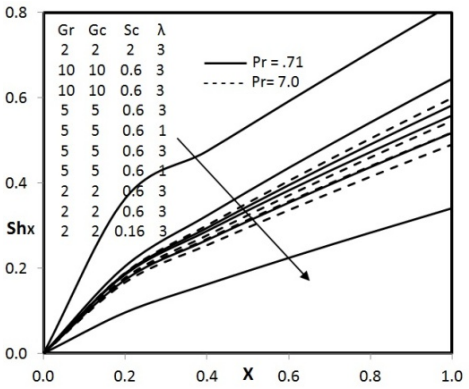

Fig. 9. Local Sherwood number.

The trend is opposite in average Nusselt number $\overline{Nu}$ with respect to *Sc*, *Gr* and *Gc*. From Fig. 11, it is seen that in the initial time steps, the rate of heat transfer is same for constant *Gr* and *Gc*. This reveals that initially heat transfer is due to conduction only. The average Nusselt number increases for increasing value of λ. usually a larger Nusselt number corresponds to more active convection. The rate of heat transfer increases for higher values of *Pr*.

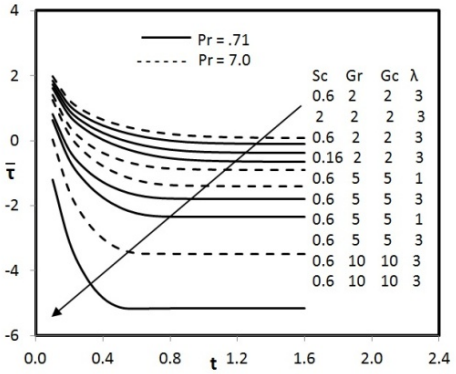

Fig. 10. Average skin friction.

In Fig. 12, the average Sherwood number is constant initially for fixed values of *Sc*. This reveals that there is only mass diffusion in the initial time level. It is observed that Sherwood number increases with t and after certain lapse of time they are steady throughout the transient period. Larger values of *Sc* give rise to higher values of Sherwood numbers. The rate of mass transfer increases with increasing *Gr*, *Gc* and *Sc*.

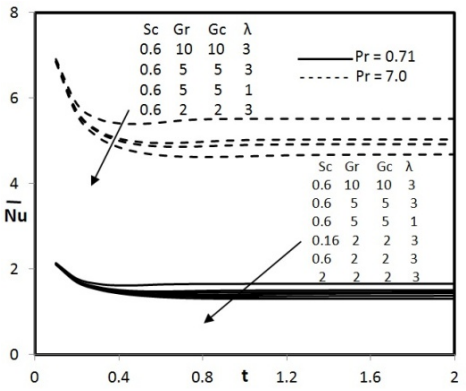

Fig. 11. Average Nusselt number.

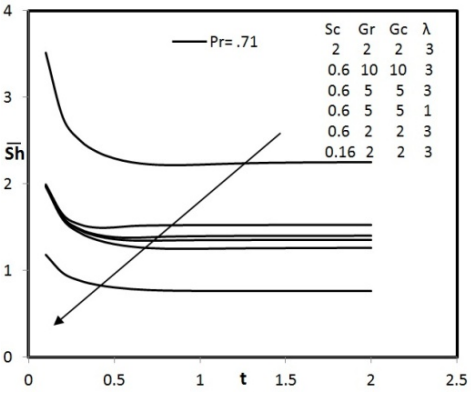

Fig. 12. Average Sherwood number.

6. CONCLUSIONS

A Numerical analysis is performed to study the free convective flow on a continuously moving semi-infinite vertical cylinder in the presence of porous medium. The dimensionless governing equations are solved by finite difference scheme of Crank-Nicolson type. The fluids considered are both air and water. The effect of Prandtl number, thermal Grashof number, modified Grashof number, Schmidt number and permeability of the porous medium are studied. Conclusions of the study are as follows:

1. As the permeability parameter λ increases, the transient velocity profile increases whereas the temperature and the concentration profiles decreases.
2. The velocity profile increases for increasing values of *Gr*, *Gc* and decreasing values of *Sc*.
3. Temperature increases with decreasing values of *Gr*, *Gc*, *Pr* and increasing values of *Sc*.
4. Concentration increases for decreasing value of *Gr*, *Gc* and *Sc*.
5. The time required to reach the steady-state temperature and concentration is higher for larger values of *Pr*.

6. The local as well average shear stress increases with increasing value of *Sc* and decreasing values of *Gr*, *Gc*. The trend is opposite in local and average heat transfer rate.

7. The local as well as average mass transfer rate increases with increasing values of *Sc* and *Gr* and *Gc*.

8. The local as well as average skin friction, Nusselt number and Sherwood number increases for increasing value of permeability parameter λ. It is observed that the skin friction values are negative at small values *Sc* indicating that separation of flow may occur at the cylinder.

9. The rate of heat transfer increases for higher values of *Pr*.

ACKNOWLEDGEMENT

The authors would like to thank the reviewers and editors for their valuable comments and suggestions.

REFERENCES

Akyildiz, T., F. Hamid Bellout and K. Vajravelu (2006). Diffusion of chemically reactive species in a porous medium over a stretching sheet. *Journal of Mathematical Analysis and Applications* 320(1), 322-339.

Ashorynejad, H. R., M. Sheikholeslami, I. Pop and D. D. Ganji (2013). Nanofluid flow and heat transfer due to a stretching cylinderin the presence of magnetic field. *Heat Mass Transfer* 49, 427-436.

Bejan, A. and K. R. Khair (1985). Heat and mass transfer by natural convection in porous medium. *International Journal of Heat and Mass transfer* 28(5), 908-918.

Bottemanne, F. A. (1972). Experimental results of pure and simultaneous heat and mass transfer by free convection about a vertical cylinder for *Pr* = 0.71 and *Sc* = 0.63. *Applied Scientific Research* 25(1), 372-382.

Carnahan, B., H. A. Luther and J. O. Wilkes (1969). *Applied Numerical Methods*. John Wiley and Sons, New York.

Chamkha, A. J. and S. E. Ahmed (2011). Similarity Solution for Unsteady MHD Flow near a Stagnation Point of a Three Dimensional Porous Body with Heat and Mass Transfer, Heat Generation/Absorption and Chemical Reaction. *Journal of Applied Fluid Mechanics* 4(1), 87-94.

Chamkha, A., R. S. Reddy Gorla and K. Ghodeswar (2011). Non-similar Solution for Natural Convective Boundary Layer Flow Over a Sphere Embedded in a Porous Medium Saturated with a Nanofluid. *Transport in Porous Medium* 86, 13-22.

Chen, T. S. and C. F. Yuh (1980). Combined heat and mass transfer in natural convection along a vertical cylinder. *International Journal of Heat and Mass Transfer* 23(4), 451-461.

Cheng, C. Y. (2010). Soret and Dufour effects on free convection boundary layer over a vertical cylinder in a saturated porous medium. *International Communications in Heat and Mass Transfer* 37(7), 796-800.

Ganesan, P. and H. P. Rani (2000). On diffusion of chemically reactive species in convective flow along a vertical cylinder. *Chemical Engineering and Processing: Process Intensification* 39(2), 93-105.

Ganesan, P. and P. Loganathan (2001). Unsteady natural convective flow past a moving vertical cylinder with heat and mass transfer. *Heat and Mass Transfer* 37(1), 59-65.

Hamad, M. A. A. and M. Ferdows (2012). Similarity solution of boundary layer stagnation-point flow towards a heated porous stretching sheet saturated with a nanofluid with heat absorption/generation and suction/blowing: A lie group analysis. *Communications in Nonlinear Science and Numerical Simulation* 17(1), 132-140.

Javaherdeh, K., M. M. Nejad and M. Moslemi (2015). Natural convection heat and mass transfer in MHD fluid flow past a moving vertical plate with variable surface temperature and concentration in a porous medium. *Engineering Science and Technology, an International Journal* 1-9.

Kuiken, H. K. (1974). The Thick free-convective boundary-layer along a semi infinite isothermal vertical cylinder. *Journal of Applied Mathematics and Physics (ZAMP)* 25(4), 497-514.

Kumari, M. and G. Nath (1999). Development of two-dimensional boundary layer with an applied magnetic field due to an impulsive motion. *Indian Journal of pure and applied mathematics* 30(7), 695-708.

Merkin, J. H. (1977). Free convection from a vertical cylinder embedded in a saturated porous medium. *Acta Mechanica* 62(1-4), 19-28.

Minkowycz, W. J. and P. Cheng (1976). Free convection about a vertical cylinder embedded in a porous medium. *International Journal of Heat and Mass transfer* 19(7), 805-813.

Mukhopadhyay, S. (2012). Mixed convection boundary layer flow along a stretching cylinder in porous medium. *Journal of Petroleum Science and Engineering* 96, 73-78.

Mukhopadhyay, S. and A. Ishak (2012). Mixed Convection Flow along a Stretching Cylinder in a Thermally Stratified Medium. *Journal of Applied Mathematics* Article 8.

Na, T. Y. and I. Pop (1983). Free convection flow past a vertical flat plate embedded in a

saturated porous medium. *International Journal of Engineering Science* 21(5), 517-526.

Narayana, S., B. Venkateswarlu and S. Venkataramana (2015). Thermal Radiation and Heat Source Effects on a MHD Nanofluid past a Vertical Plate in a Rotating System with Porous Medium. *Heat Transfer–Asian Research* 44(1), 1-19.

Noghrehabadi, A., M. Ghalambaz and A. Ghanbarzadeh (2014). Effects of Variable Viscosity and Thermal conductivity on Natural Convection of Nanofluids Past a Vertical Plate in Porous Media. *Journal of Mechanics* 30(3), 265-275.

Patil, P. M. and P. S. Kulkarni (2008). Effects of chemical reaction on free convective flow of a polar fluid through a porous medium in the presence of internal heat generation. *International Journal of Thermal Sciences* 47(8), 1043-1054.

Postelnicu, A. (2004). Influence of a magnetic field on heat and mass transfer by natural convection from vertical surfaces in porous media considering Soret and Dufour effects. *International Journal of Heat and Mass transfer* 47(6-7), 1467-1472.

Raptis, A., G. Tzivanidis and N. Kafousias (1981). Free convection and mass transfer flow through a porous medium bounded by an infinite vertical limiting surface with constant suction. *Lettersin Heat and Mass Transfer* 8(5), 417-424.

Rohni, A. M., S. Ahmad, J. H. Merkin and I. Pop (2013). Mixed Convection Boundary-Layer Flow Along a Vertical Cylinder Embedded in a Porous MediumFilled by a Nanofluid. *Transport Porous Medium* 96, 237-253.

Singh, P., J. K. Misra and K. A. Narayan (1986). A mathematical analysis of unsteady flow and heat transfer in a porous medium. *International Journal of Engineering Science* 24(3), 277-287.

Takhar, H. S., A. J. Chamkha and G. Nath (2001). Unsteady three-dimensional MHD-boundary-layer flow due to the impulsive motion of a stretching surface. *Acta Mechanica* 146, 59-71.

Vajravelu, K., K. V. Prasad and Ch. O. Ng (2013). Unsteady convective boundary layer flow of a viscous fluid at a vertical surface with variable fluid properties. *Nonlinear Analysis: Real World Applications* 14, 455-464.

Velusamy, K. and V. K. Garg (1992). Transient natural convection over a heat generating vertical cylinder. *International journal of heat and mass transfer* 35(5), 1293-1306.

Yadav, R. S. and P. R. Sharma (2014). Effects of Porous Medium on MHD Fluid Flow along Stretching Cylinder. *Annals of Pure and Applied Mathematics* 6(1), 104-113.